Acta Oceanol. Sin., 2024, Vol. 43, No. 10, P. 74–85
https://doi.org/10.1007/s13131-024-2418-4
http://www.aosocean.com
E-mail: ocean2@hyxb.org.cn

The significant role of submarine groundwater discharge in an Arctic fjord nutrient budget

Xueqing Yu[1, 2], Jian'an Liu[3]*, Zhuoyi Zhu[4, 5], Xiaogang Chen[6], Tong Peng[2], Jinzhou Du[2]

[1] College of Geography and Environmental Science, Key Laboratory of Tropical Island Land Surface Processes and Environmental Changes of Hainan Province, Hainan Normal University, Haikou 571158, China

[2] State Key Laboratory of Estuarine and Coastal Research, East China Normal University, Shanghai 200241, China

[3] State Key Laboratory of Marine Resource Utilization in South China Sea, Hainan University, Haikou 570228, China

[4] Shanghai Key Laboratory of Polar Life and Environment Sciences, School of Oceanography, Shanghai Jiao Tong University, Shanghai 200030, China

[5] MNR Key Laboratory for Polar Science, Polar Research Institute of China, Shanghai 200136, China

[6] Key Laboratory of Coastal Environment and Resources of Zhejiang Province, School of Engineering, Westlake University, Hangzhou 310024, China

Received 5 July 2024; accepted 4 November 2024

Abstract

Under global climate change, water flow and related nutrient biogeochemistry in the Arctic are changing at an unprecedented rate, and potentially affect nutrient cycling in the Arctic Ocean. However, nutrient fluxes via submarine groundwater discharge (SGD) are potentially important yet poorly understood in the Arctic. Here we quantified that nutrient fluxes through radium-derived SGD were three orders of magnitude higher than those from the local river and constituted 25%–96% of the total nutrient inputs into the Kongsfjorden. These large groundwater nutrient fluxes with high NIN/DIP molar ratio (average 99) may change the biomass and community structure of phytoplankton. Meanwhile, combining other SGD study cases around the Arctic region, SGD rates tend to increase over the past three decades, possibly on account of the effects of global warming. The SGD-derived nutrient may cause the increase of net primary productivity in the Arctic Ocean. The results will provide important basic data for land-ocean interactions in the typical fjord of the Arctic under the influence of global warming.

Key words: Arctic, submarine groundwater, nutrient biogeochemistry, primary productivity, radium isotopes, global climate change

Citation: Yu Xueqing, Liu Jian'an, Zhu Zhuoyi, Chen Xiaogang, Peng Tong, Du Jinzhou. 2024. The significant role of submarine groundwater discharge in an Arctic fjord nutrient budget. Acta Oceanologica Sinica, 43(10): 74–85, doi: 10.1007/s13131-024-2418-4

1 Introduction

The Arctic region is one of the most important places to study climate change and climate records because it is highly vulnerable to climate change (Peterson et al., 2002; Polyakov et al., 2012; Semenov et al., 2020). Under the influence of global warming amplification, the rate of temperature increases in the Arctic subsurface is about two times as much as that of the middle and low latitudes, which contributes to rapid and widespread permafrost thawing (Collins et al., 2013; Guimond et al., 2022; Smith et al., 2007; Walvoord and Striegl, 2007). The processes of glacial meltwater and sea ice melting in summer make large amount of fresh water enter the Arctic Ocean, one way through the riverine, and others directly fall into the sea by the frontal interface of glaciers and surface seas. This fresh water with the matter and energy balance changing has a significant impact on the ecological environment (Bridgestock et al., 2021a; Kipp et al., 2018; Vonk et al., 2012). In addition, freshwater from glacier melting can be also infiltrated into the aquifers and then enters the ocean through coastal groundwater (Bridgestock et al., 2021a; Dimova et al., 2015; Kipp et al., 2018; Lecher, 2017). Except that temperature rises, the interaction between coastal groundwater and surface water in the Arctic Ocean may cause heat transfer to sediments or deeper soil layers along the Arctic Ocean coastline, leading to the permafrost melting. This phenomenon would enhance the flux of terrestrial freshwater into the coastal area and its-derived nutrient input to the sea, which results in a change in the structure and composition of the plankton community (Dimova et al., 2015; Lecher et al., 2016a, b; Piquet et al., 2014).

Submarine groundwater discharge (SGD) is defined as the water flow (including fresh SGD and saline SGD) on the continental margin from the seabed to the coastal ocean, regardless of fluid composition or driving force (Burnett et al., 2003). SGD also exists in the Arctic and is very susceptible to the effect of global warming. It is unique in that glacial meltwater permeates into underground aquifers and discharges as SGD into coastal waters (Charkin et al., 2017). Most importantly, SGD also has been widely recognized as a significant mechanism for transporting related solutes into the ocean (Lecher, 2015; Liu et al., 2017; Moore,

Foundation item: The National Natural Science Foundation of China under contract Nos 41976040, 41676188, 42106043 and 42006152; the Innovation Base for Estuarine and Coastal Water Security 2.0 from the Ministry of Science and Technology of P.R. China under contract No. BP0820020.

*Corresponding author, E-mail: liujianan@hainanu.edu.cn

2010; Rodellas et al., 2015; Santos et al., 2021). Specifically, SGD-derived solutes have been shown to be comparable to rivers, benthic sediments and atmospheric inputs in coastal areas on regional and global scales (Hwang et al., 2010; Kim et al., 2005; Rodellas et al., 2015; Santos et al., 2021; Swarzenski, 2007). As a naturally occurring radioactive tracer, radium (Ra) isotopes (^{224}Ra, ^{223}Ra, ^{228}Ra, and ^{226}Ra) have widely varying half-lives (3.66 d, 11.4 d, 5.75 a, and 1 602 a, respectively). Radium tracing is one of the most effective methods for quantifying SGD flux into coastal waters within different temporal and spatial scales (Garcia-Orellana et al., 2021; Moore, 1996).

The Arctic region has always been an under-studied area of SGD, with a few of those trying to understand the nature of groundwater discharge and its impact on aquatic ecosystems. In particular, because of the impact of climate change, the large area of permafrost and floating ice melts, the SGD in the Arctic region (especially the SGD from the permafrost) need for more attention. Lecher (2017) summarized SGD studies in the Arctic, which showed the important role of SGD on nutrient and trace elements supply (Dimova et al., 2015; Lecher, 2015; Lecher et al., 2016a, b). Kipp et al. (2018) found that ^{228}Ra activities in the surface waters of the central Arctic Ocean increased due to shelf input into the central basin, revealing the transport of elevated concentrations of nutrient and dissolved organic carbon, which can through shelf sediments and/or SGD. Connolly et al. (2020) presented substantial fluxes of dissolved organic matter delivered by supra-permafrost groundwater to the Alaska Beaufort Sea, and the fluxes are expected to increase in a warming Arctic. As a result, SGD is expected to become an increasing source of nutrient in the Arctic Ocean as permafrost thaws, where the nutrient cycling is undergoing major changes that have the potential to affect biological productivity and species composition in the Arctic waters (Kipp et al., 2018).

However, there are few studies on the effects of SGD on the nutrient structures in the Arctic region. Therefore, the research on the SGD-associated nutrient under the influence of global climate change has become an attention-grabbing hotspot in the Arctic. Rapid changes in the ice cover of Svalbard make it one of the key regions for the interaction of Arctic ice dynamics and climate change on geological time scales (Kim et al., 2022; Polyakov et al., 2012). The accelerated shrinkage of the cryosphere has attracted the attention of researchers on the potential effects of hydrology, fluid dynamics, sediments and bio-communities from land to ocean (Hodson et al., 2019; Kim et al., 2022; Yoshikawa and Harada, 1995). So far, most studies of freshwater discharges in Svalbard have focused on local rivers and glacier meltwater discharge (Haldorsen and Heim, 1999; Kim et al., 2022; Olichwer et al., 2013), less attention was paid to the impact of SGD on the coastal environment. The early Holocene was a relatively warm period with a large influx of warm Atlantic water, leading to the formation of sea ice and the reduction of glacial extent in the Kongsfjorden (Chen et al., 2016; Kim et al., 2022; Peral et al., 2022). Land-ocean interactions are key to understand and predict hydrology and nutrient cycling in Svalbard during past, present and future under global climate change.

Here, we analyze Ra and nutrient concentrations in seawater, river and coastal groundwater around the Kongsfjorden, a typical Arctic fjord. The goals of our study are to (1) use ^{226}Ra and ^{228}Ra mass balance models, including uncertainty analysis, to estimate SGD and its derived nutrient fluxes in Kongsfjorden; (2) build nutrient budget in Kongsfjorden to assess the environmental impacts of SGD; (3) evaluate SGD-derived nutrient fluxes around the Arctic Ocean with the support of available literature, hope to contribute to a deeper understanding and better prediction of global warming impacts on SGD which may affect the Arctic Ocean ecosystem.

2 Materials and methods

2.1 *Study area*

The Kongsfjorden (78.49°–79.24°N, 10.89°–13.45°E) is located in the northwestern part of the Svalbard Islands (Fig. 1). Only one major river, the Bayelva River flows into the fjord, with a length of ~4 km and a small runoff of 8.18×10^4 m^3/d (Zhu et al., 2016), the other rivers have less runoff and generally do not melt into the fjord in summer, so we ignore their contributions in our following SGD calculation. Due to the influence of the North Atlantic Warm Current flowing through the archipelago, the temperature is much milder than in other parts of the Arctic, with an average annual temperature of –4 ℃, but it's usually above freezing between July and September (https://www.pric.org.cn/). The mean monthly precipitation here was 48 mm, both rain and snow may occur in the Kongfjorden at any time throughout the year (Hop and Wiencke, 2019). The maritime climate of the archipelago is more pronounced, and the pelagic ecosystem is sensitive to the effects of the Atlantic and Arctic Ocean, while the benthic ecosystem is mainly affected by long-term changes in glacial runoff and sedimentation (Svendsen et al., 2002). An irregular diurnal tide exists in this region, with a mean tidal range of 200 cm (Sinha et al., 2017). Sediment in Kongsfjorden exhibits glacial till characteristics and the major sediment types were moraine lacking silt and mud, moraine containing sand, and moraine lacking sand (Sinha et al., 2017).

Seasonal sea ice is an important feature of Kongsfjorden, significantly affecting the physical environment and ecosystem. The inner fjord is usually covered with seasonal ice, initially forming between December and March and continuing through April to June. Seasonal ice has been confined to the northern inner fjords over the past decades (Hop and Wiencke, 2019; Polyakov et al., 2012; Zhu et al., 2016). The maximum sea ice sonic thickness is about 0.6 m or more, and the snow thickness on the fjord has decreased by about 0.2 m in the last decade (Hop and Wiencke, 2019). Warmer horizontal Atlantic currents entering the fjord also contributed to reducing rapid ice formation. Seasonal dynamics of sea ice extent have important implications for pelagic and benthic production as well as for seabirds and marine mammals in the marine ecosystem of Kongsfjorden (Hop and Wiencke, 2019). The landscape around Kongsfjorden is influenced by glacial, and during the summer, there are many places where glacial melt not only directly enters the fjord, but also feeds into the rivers and underground aquifers, which are the main source of fresh water for the Kongsfjorden (Kuliński et al., 2014).

2.2 *Sampling collection*

Field research was conducted in the Kongsfjorden (Fig. 1) during summer between late August and early September 2017 with the sampling locations shown in Fig. 1. All the Ra samples were obtained from the surface water (~60 L) at a depth of ~1 m using a submerged pump. Moreover, coastal groundwater (porewater) and river water were collected as endmembers for the Kongsfjorden. Porewater samples (n = 2, ~20 L, <2 m) were collected within 50 m offshore and in the active area of permafrost in summer with a push-point piezometer using a peristaltic pump (Moore et al., 2006). River water (40 L) was collected using an organic glass hydrophore. At the same time, suspended particulate matter is obtained by collecting river water (i.e., RW in Fig. 1) and filtering it using a glass fiber membrane with a pore size of 0.45 μm. The salinity, temperature, pH and dissolved oxygen

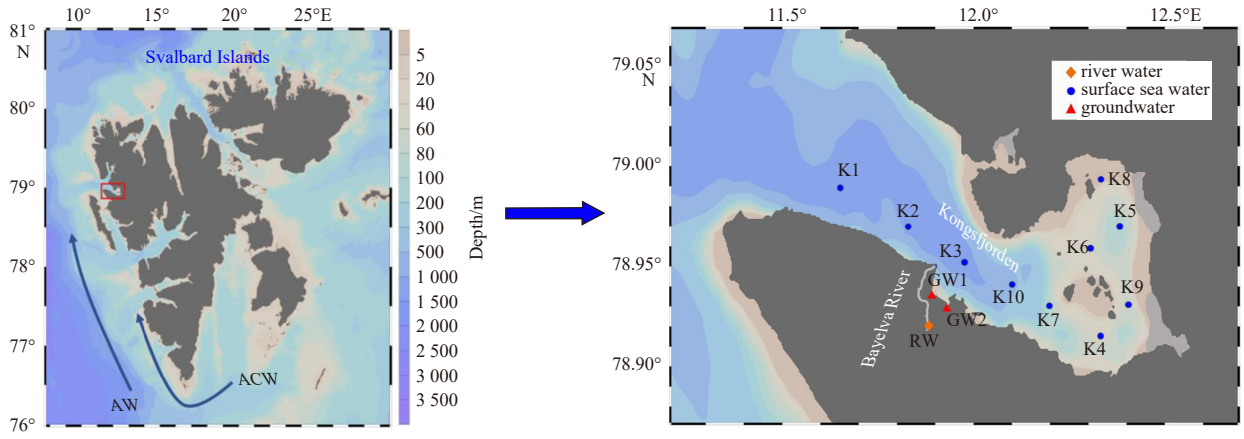

Fig. 1. Locations of the Kongsfjorden and sampling station during 2017. Blue circles, orange diamonds and red triangles represent surface water, river water and groundwater, respectively. Blue arrows indicate ocean currents of Atlantic Water (AW) and Arctic Coastal Water (ACW) (Zhu, 2022).

were determined *in situ* using a conductance-temperature-depth sensor (Multi 3430 WTW, Germany). The Ra samples were collected into plastic buckets, passed slowly through columns filled with ~20 g MnO_2 fibers and then were stored for measurement (Moore and Arnold, 1996). Samples for nutrient concentrations analyses (~60 mL) were first filtered through 0.45 μm sterile cellulose acetate filters, rinsed the low-density polyethylene bottles (these bottles were 60 mL nominal size and pre-cleaned with 1 mol/L hydrochloric acid) with filtered water sample, then filtered water samples were collected and stored in dark at –20℃.

2.3 *Desorption experiment of suspended particulate matter*

To estimate the Ra desorbed from suspended particulate matter, we performed desorption experiments using suspended particulate matter. The dried suspended particulate matter (0.5 g) was suspended in 5 L of Ra-free seawater with salinity 33. Mixed the seawater and suspended particulates for 2 h using an electric mixer with the appropriate speed. The suspension was allowed to settle and the particulates were separated from the seawater using a 0.45 mm filter. Ra in the filtrate was enriched on MnO_2 fibers and brought back to the laboratory for measurement.

2.4 *Analytical methods*

Upon back to the laboratory, the MnO_2 fibers were ashed at 800℃ for 8 h, homogenized, loaded into a plastic vial to a height of ~30 mm (same height for the standards) and sealed with an epoxy sealant. After aging to allow ingrowth of ^{222}Rn, ^{226}Ra and ^{228}Ra were determined by a calibrated HPGe gamma spectrometry (Ortec, GWL-120-15XLB-AWT) in our laboratory, which the detector was calibrated to ensure its accuracy using certified reference materials (batch number: 08121) obtained from the National Institute of Metrology, China (Liu et al., 2021). Generally, ^{226}Ra activities were obtained using ^{214}Pb (295 keV and 352 keV) and ^{214}Bi (609 keV) peaks, while ^{228}Ra activities were obtained using the 338 keV and 911 keV peaks of ^{228}Ac.

The samples for nutrient concentrations were analyzed for the measurement of dissolved nitrate (NO_3^-), nitrite (NO_2^-), ammonium (NH_4^+), dissolved inorganic phosphorus (DIP) and dissolved silicate (DSi) using an autoanalyzer (Model: Skalar SANplus; Liu et al., 2009). The concentration of dissolved inorganic nitrogen (DIN) is expressed as the sum of NO_2^-, NO_3^-, and NH_4^+ concentrations. The analytical precisions of NO_2^-, NO_3^-, NH_4^+, PO_4^{3-} and Si $(OH)_4$ were all better than 5% and the detection limits were 0.01 μmol/L, 0.05 μmol/L, 0.05 μmol/L, 0.01 μmol/L and 0.1 μmol/L, respectively (Liu et al., 2022).

3 Results

3.1 *Hydrographic parameters distributions*

In the surface water of the Kongsfjorden, the salinity ranged from 30.8 to 32.3, with an average of 31.5 (n = 9). The temperature changed from 3.70℃ to 7.30℃, with an average of 6.01℃. The dissolved oxygen (DO) changed from 12.6 mg/L to 13.4 mg/L and pH ranged from 8.3 to 8.6 (Table 1). Surface water showed higher temperature and lower salinity in the nearshore waters. Station K1 is the farthest offshore station with a maximum salinity of 33.2, which we selected as the open-sea water endmember. To explore the vertical mixing degree of water, we selected K2, K3, and K5 profiles for observation, and a thermocline is observed in the upper 10 m layer of this fjord (Fig. 2). In the coastal groundwater, the salinity ranged from 0 to 16.5, with a mean value of 8.25. The temperature ranged from 3.5℃ to 4.0℃, with a mean value of 3.8℃. The DO concentration ranged from 0.2 mg/L to 12.5 mg/L and pH changed from 8.1 to 8.3. In the river water of the Kongsfjorden, salinity and temperature were 0.2 and 1.9℃, DO and pH were 13.0 mg/L and 8.6, respectively.

3.2 *^{226}Ra and ^{228}Ra distributions*

The activities of the ^{226}Ra and ^{228}Ra isotopes in the Kongsfjorden at various stations are presented in Table 1. In surface water, ^{226}Ra and ^{228}Ra activities ranged from (2.1 ± 0.20) Bq/m^3 to (3.3 ± 0.20) Bq/m^3 and (1.7 ± 0.27) Bq/m^3 to (3.1 ± 0.45) Bq/m^3, respectively. In coastal groundwater, ^{226}Ra activities varied from (6.1 ± 0.28) Bq/m^3 to (8.6 ± 0.28) Bq/m^3 while ^{228}Ra activities varied from (8.6 ± 0.30) Bq/m^3 to (19.2 ± 0.37) Bq/m^3. The main river entering Kongsfjorden is the Bayelva River, ^{226}Ra and ^{228}Ra activities were (2.7 ± 0.28) Bq/m^3 and (3.5 ± 0.436) Bq/m^3, respectively. Since the other rivers were barely discharged into the bay during the sampling period, the following discussion will be based solely on data from the Bayelva River station. In open-sea water of the Kongsfjorden, the ^{226}Ra and ^{228}Ra activities were (2.0 ± 0.28) Bq/m^3 and (1.5 ± 0.48) Bq/m^3, respectively. Figure 3 shows the distribution of activities of Ra isotopes in different sources of the Kongsfjorden. It can be seen that the Ra activities of groundwater were 2 to 4 times greater than those in surface water and river water, providing evidence that groundwater may

Table 1. Concentrations of ^{226}Ra, ^{228}Ra, nutrient and other parameters in all samples collected in the Kongsfjorden

Station	Latitude	Longitude	Temp/℃	Salinity	pH	DO/ (mg·L^{-1})	^{228}Ra/ (Bq·m^{-3})	^{226}Ra/ (Bq·m^{-3})	DIN/ (μmol·L^{-1})	DIP/ (μmol·L^{-1})	DSi/ (μmol·L^{-1})
	Seawater										
K2	78.968 7°N	11.829 2°E	3.7	31.7	8.3	12.9	2.4 ± 0.37	2.2 ± 0.32	5.17	0.234	0.591
K3	78.951 8°N	11.972 7°E	6.6	30.8	8.5	13.1	3.1 ± 0.45	2.5 ± 0.30	7.58	0.073	1.50
K4	78.916 1°N	12.330 8°E	6.7	31.3	8.5	13.0	2.3 ± 0.32	2.9 ± 0.25	–	–	–
K5	78.970 5°N	12.381 1°E	7.3	32.3	8.4	12.7	2.0 ± 0.25	2.4 ± 0.22	7.68	0.103	1.99
K6	78.959 2°N	12.302 6°E	6.5	32.2	8.4	12.8	1.7 ± 0.27	2.3 ± 0.22	–	–	–
K7	78.930 3°N	12.201 4°E	6.5	31.5	8.5	13.4	3.1 ± 0.25	3.3 ± 0.20	–	–	–
K8	78.993 6°N	12.330 0°E	6.5	30.9	8.5	13.3	2.4 ± 0.25	2.4 ± 0.18	–	–	–
K9	78.930 2°N	12.400 0°E	4.9	31.4	8.3	12.7	2.3 ± 0.40	2.8 ± 0.32	–	–	–
K10	78.940 5°N	12.101 3°E	5.4	31.1	8.6	12.6	1.9 ± 0.30	2.1 ± 0.20	–	–	–
	Groundwater										
GW1	78.930 0°N	11.930 7°E	4.0	0.0	8.1	0.2	8.6 ± 0.30	6.1 ± 0.25	63.7	0.369	48.8
GW2	78.950 2°N	11.900 8°E	3.5	16.5	8.3	12.5	19.2 ± 0.37	8.6 ± 0.28	5.76	0.234	8.02
	River water										
RW	78.935 0°N	11.920 3°E	1.9	0.2	8.6	13.0	3.5 ± 0.43	2.7 ± 0.28	11.8	0.330	10.5
	Open sea										
K1	78.989 9°N	11.652 0°E	4.0	33.2	8.7	13.3	1.5 ± 0.48	2.0 ± 0.28	4.53	0.205	0.758

Notes: Temp: temperature; DO: dissolved oxygen concentration; Ra, DIN, DIP, DSi represent their concentrations. – represents no data.

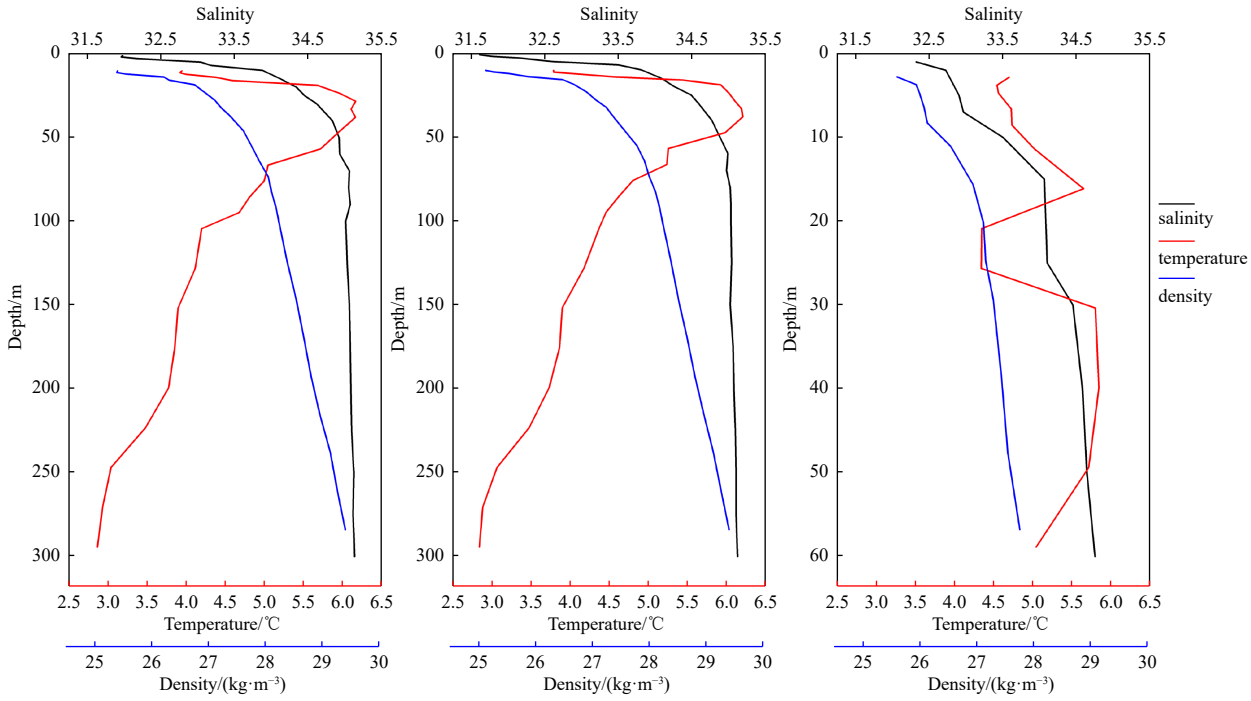

Fig. 2. Vertical distributions of salinity, temperature, and density at stations K2, K3, K5 in Kongsfjorden.

be one of the major Ra sources of the Kongsfjorden.

3.3 *Nutrient distribution*

The nutrient concentrations in different water types of the Kongsfjorden are shown in Table 1 and Fig. 4. The DIN, DIP and DSi concentrations of the surface water ranged from 5.17 μmol/L to 7.68 μmol/L, 0.07 μmol/L to 0.23 μmol/L and 0.59 μmol/L to 2.0 μmol/L, respectively. The DIN, DIP, and DSi concentrations were 11.8 μmol/L, 0.33 μmol/L, and 10.5 μmol/L in the Bayelva River, and 4.53 μmol/L, 0.21 μmol/L, and 0.76 μmol/L in the open-sea water, respectively. In coastal groundwater, the DIN, DIP, and DSi concentrations had wide ranges from 5.76 μmol/L to 63.7 μmol/L, 0.23 μmol/L to 0.37 μmol/L and 8.02 μmol/L to 48.8 μmol/L, respectively. DIN and DSi concentrations in groundwater were much higher than that in river water and surface water, while the DIP concentration in groundwater was slightly higher than that in river water and surface water. The nutrient distribution in the fjord also reflects the strong signature of groundwater inputs, while the contribution of the river is smaller.

4 Discussion

4.1 *Flushing time in the upper Kongsfjorden*

In order to estimate the SGD flux, it is necessary to know the water age of the fjord. Flushing time can provide a timescale for the accumulation of components in the water column. Assuming

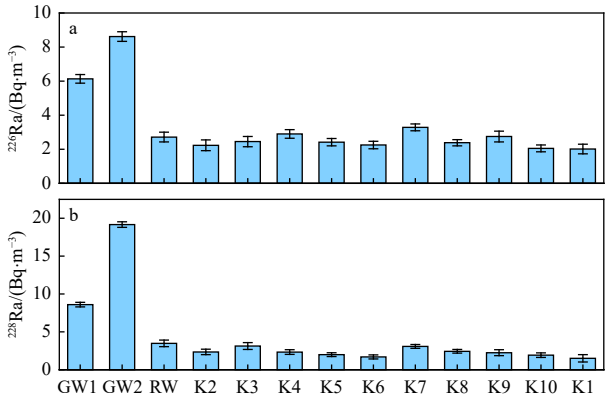

Fig. 3. The distributions of ^{226}Ra (a) and ^{228}Ra (b) activities (Bq/m^3) in the different sources of Kongsfjorden.

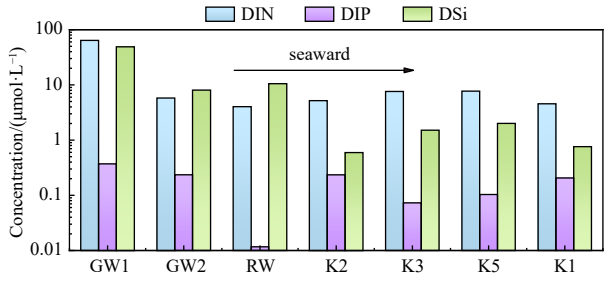

Fig. 4. The distributions of DIN, DIP and DSi concentrations (μmol/L) in the different water sources of the Kongsfjorden.

that the influence of the wind is neglected, we concerned the water volume in the upper 10 m layer above the thermocline, and the flushing time is only affected by the tide and the fresh water from the land. The flushing time (T_f, d) in the bay area can be expressed by the equation modified from Sanford et al. (1992) as follows:

$$T_f = \frac{V}{(1-b)\frac{P}{T} + D_{\mathrm{RIV}} + D_{\mathrm{GLA}}}, \tag{1}$$

$$P = \int_H^0 A\mathrm{d}z, \tag{2}$$

where V is the volume of the bay of 2.75×10^9 m^3, T is the tidal period of 0.52 d (data from https://www.tide-forecast.com/). P is the tidal prism from ebb tide to high tide bay calculated by Eq. (2), which is 5.50×10^8 m^3. b is the return flow portion from the open-sea water. A is the water surface area of the study region of 275 km^2 (Yang et al., 2022), and z is the water depth within the tidal range (H = 2.0 m; Sinha et al., 2017). D_{RIV} and D_{GLA} refer to the flows of the Bayelva River and glacier melt water during the sampling period, which are 8.18×10^4 m^3/d and 1.73×10^5 m^3/d, respectively (Torsvik et al., 2019; Zhu et al., 2016). Based on the assumptions similar to those of Moore et al. (2006), b can be estimated by the average salinity of the surface water in the Kongsfjorden divided by the salinity of open-sea water, and the value is obtained to be 0.93 here. The method is based on the physical renewal capability of the bay water (Baléo et al., 2001; Geyer et al., 2000) and obtains a single value rather than a different age range for each point. Then, we calculated the flushing time of the bay to be (39.1 ± 8.3) d.

4.2 *Radium isotopes mass balance model*

Here we used the Ra mass balance model that is based on the balance of Ra sources and sinks to obtain SGD flux. As mentioned above, a thermocline is observed in the Kongsfjorden, thus to make it more accessible and to emphasize the importance of SGD, the upper 10 m layer was used as the research object. Besides, Ra-traced SGD flux in coastal zones generally represents groundwater from shallow aquifers (Garcia-Orellana et al., 2021), and this is another reason why we chose the upper layer for our calculations. In our study area, the major inputs of Ra are from SGD, river, desorption of and glacial melt water, while the major output included two main processes: mixing between fjord water and open seawater and radioactive decay. If it is assumed that the system is in a steady state condition, the Ra mass balance model can be described as follows:

$$F_{\mathrm{RIV}} + F_{\mathrm{DES}} + F_{\mathrm{SGD}} + F_{\mathrm{GLA}} = F_{\mathrm{MIX}} + F_{\mathrm{DEC}}, \tag{3}$$

where F_{RIV}, F_{DES}, F_{SGD}, F_{GLA} and F_{DEC} represent the fluxes of Ra entering the bay through rivers, desorption of suspended particulate matters, SGD, glacial melting and decay losses, respectively. F_{MIX} represents the output of Ra via mixing with open sea water. F_{DEC} is ignored here due to the short time scale in the sampling period. After all other Ra isotope sources and sinks in Eq. (3) are available, the F_{SGD} can be calculated. And then SGD fluxes can be calculated by selecting the appropriate groundwater endmember as follows:

$$\mathrm{SGD} = \frac{F_{\mathrm{SGD}}}{[\mathrm{Ra}_{\mathrm{SGD}}]}, \tag{4}$$

where $[\mathrm{Ra}_{\mathrm{SGD}}]$ represent the appropriate groundwater endmember activity.

4.2.1 *The major input of Ra isotopes into the upper Kongsfjorden*

Ra from river input can be an important source and is usually estimated by multiplying the river flow by the Ra activities in the river water endmember. In the present study, the measured ^{226}Ra and ^{228}Ra activities were comparable to other Arctic rivers (Bullock et al., 2022). Therefore, with the activities measured in river water, the dissolved ^{226}Ra and ^{228}Ra fluxes from the river into the upper Kongsfjorden were calculated to be $(0.22 \pm 0.023) \times 10^6$ Bq/d and $(0.29 \pm 0.035) \times 10^6$ Bq/d, respectively.

Ra from desorption of suspended particulate matters in mid-salinity carried by rivers also contributed to dissolved radium in the upper water. The concentration of suspended particulate matter in the Bayelva River during our sampling period is 103 mg/L (Zhu, 2022). Based on the results of desorption experiment, the activity of ^{226}Ra and ^{228}Ra desorbed by particle matters is (0.20 ± 0.16) Bq/g and (0.18 ± 0.14) Bq/g. By multiplying the activity of desorbed radium with the sediment runoff of 8.42×10^3 kg/d, the desorbed radium flux input by the Bayelva River can be calculated as $(0.17 \pm 0.14) \times 10^7$ Bq/d for ^{226}Ra and $(1.49 \pm 0.96) \times 10^6$ Bq/d for ^{228}Ra.

The local geologic structure is permeable (Zhu et al., 2016), a portion of glacial meltwater in summer flows into rivers and tectonic layers of permafrost and drains into bays (Charkin et al., 2011), and the other part is directly discharged into the fjord through the active part of the glacier front. The meltwaters from Kongsbreen and Blomstrandbreen input into the fjord is about 1.73×10^5 m^3/d (Torsvik et al., 2019). The activities of ^{228}Ra and ^{226}Ra from meltwater are (6.42 ± 0.27) Bq/m^3 and (0.50 ±

0.058) Bq/m^3 (Linhoff et al., 2020). So the Ra fluxes from meltwater can be calculated as (0.86 ± 0.10) × 10^6 Bq/d for ^{226}Ra and (1.11 ± 0.46) × 10^7 Bq/d for ^{228}Ra.

4.2.2 *The major output of Ra isotopes into the Kongsfjorden*

The Ra loss of exchange between open-sea water and the inner bay water is an important Ra sink in the bay. The loss of Ra via mixing with open seawater is described by Eq. (5) (Kim et al., 2011; Luo et al., 2014):

$$F_{\mathrm{MIX}} = \frac{Ra - Ra_{\mathrm{O}} \times b - (1-b) \times Ra_{\mathrm{RIV}}}{T_f} \times V, \tag{5}$$

where Ra is the average Ra activities (Bq/m^3) measured in bay water, for ^{226}Ra and ^{228}Ra, the values were (2.52 ± 0.24) Bq/m^3 and (2.33 ± 0.32) Bq/m^3, respectively. Ra_{O} and Ra_{RIV} are the Ra activities (Bq/m^3) measured in open-sea water and river water, respectively. With other parameters mentioned above, the mixed loss fluxes (F_{MIX}) of ^{226}Ra and ^{228}Ra in Kongsfjorden were (0.33 ± 0.12) × 10^8 Bq/d and (0.38 ± 0.083) × 10^8 Bq/d, respectively.

4.2.3 *SGD flux in the upper Kongsfjorden*

Based on the Ra isotopes mass balance model, the ^{226}Ra and ^{228}Ra fluxes through SGD input can be determined to be (0.30 ± 0.11) × 10^8 Bq/d and (0.25 ± 0.068) ×10^8 Bq/d, which accounted for approximately 91.4% and 65.7% of the total sources into the upper Kongsfjorden, respectively. Commonly, the selection of an appropriate end-member is the main source of uncertainty in SGD estimates (Burnett et al., 2008; Cho and Kim, 2017; Cerdà-Domènech et al., 2017). In this study, although only two coastal groundwater samples were obtained, considering the high ^{226}Ra and ^{228}Ra activities in groundwater, they both have the potential to be the significant Ra source to coastal water. At the same time, the groundwater sampling stations are located within 50 m offshore and are located in the area where the permafrost is active in summer, so the permafrost and glacier will melt in a large area during our sampling period (McGovern et al., 2022), which provides a conduit between the coastal aquifer and the fjord and then promotes the SGD. Thus, our limited groundwater samples are also representative to a certain extent. In order to avoid the uncertainty caused by the difference between the endmember values, we use high value (conservative value) to represent the general level of coastal groundwater. The groundwater endmember values were (8.62 ± 0.28) Bq/m^3 for ^{226}Ra and (19.2 ± 0.37) Bq/m^3 for ^{228}Ra. Then, according to Eq. (9), the SGD fluxes are calculated to be (3.45 ± 0.39) × 10^6 m^3/d and (1.28 ± 1.01) × 10^6 m^3/d by ^{226}Ra and ^{228}Ra, respectively. SGD fluxes calculated by different methods are within the same order of magnitude. Therefore, SGD fluxes ranged from 1.28 × 10^6 m^3/d to 3.45 × 10^6 m^3/d, with an average of (2.37 ± 0.70) × 10^6 m^3/d. We can see that SGD fluxes were ~29 times the flow of the local river and ~14 times the flow of the glacier meltwater during our sampling period. It should be noted that our estimated SGD flux is not just a freshwater flux, but a mixture of seawater and terrestrial water mixtures from the coastal aquifer.

Generally, different subterranean estuaries have different forcing conditions, such as tides, waves, freshwater gradients, density gradients, and seasons (Michael et al., 2005; Santos et al., 2012). We summarized the typical SGD fluxes entering the coastal regions in different parts of the Arctic (the details are shown in Section 4.4), indicating that the SGD rate in Kongsfjorden is within the SGD rates of the Arctic coastal system. Due to the special form of groundwater in the Arctic, tidal range research in the study area is relatively small, and the melting of the permafrost and glaciers in summer is intensifying. Arctic glacial meltwater can be transported from the near shore to the central area of the Arctic Ocean, one part is directly entering the ocean, and the rest of it can be infiltrated into the aquifers and enter the ocean as groundwater (Kipp et al., 2018), so parts of the estimated SGD flux overlaps with glacier meltwater discharge, but it is difficult for us to quantitative separate from them. Therefore, the SGD in the coastal areas of the Arctic Ocean occurs primarily during the summer, and, undoubtedly, the SGD flux is also very sensitive to the effects of global warming in the Arctic region.

In this study, all the uncertainties are estimated based on the errors of the measured data, and then the basic rules of error propagation are widely used to estimate the uncertainties in SGD (Sadat-Noori et al., 2015). From the Ra isotope mass balance model, many factors affect the SGD calculation. Changes (10%) in our estimated flushing time resulted in 11.0%–13.4% uncertainty in SGD flux estimates, indicating that flushing time in the upper Kongsfjorden is still sensitive to SGD flux calculations. Furthermore, the river input does not strongly affect the Ra mass balance model due to its low value. Besides, SGD flux calculation is usually sensitive to Ra activity in coastal groundwater. In the present study, if activities of ^{226}Ra and ^{228}Ra in coastal groundwater endmembers changed by 10%, it would result in SGD uncertainty of 9.1%–11.1%. Sampling from aquifers of different geological formations results in variations in endmember values, so it is normal to observe variations of tens of Bq/m^3 in the Ra activity of groundwater. Meanwhile, it shows that SGD flux in such a typical Arctic fjord remains at a relatively high level, which needs more attention from scientists.

4.3 *SGD impacts the nutrient budget in the upper Kongsfjorden*

4.3.1 *SGD-derived nutrient fluxes*

Previous studies have shown that SGD is a significant source of nutrient in the coastal waters (e.g., Oehler et al., 2018; Santos et al., 2021). Even a small volumetric SGD will also transport high-flux nutrient, thus resulting in important ecological and environmental effects. The classical method of SGD-derived nutrient fluxes was multiplying the SGD flux by the nutrient concentrations in the groundwater endmember, which has been widely used in previous studies (Kim et al., 2005; Luo et al., 2014; Luo and Jiao, 2016; Moore et al., 2006; Wang et al., 2017, 2018). So to obtain a comparable estimate of nutrient from SGD inputs to the Kongsfjorden, we also use the typical approach in our study. The nutrient concentrations selected in the coastal groundwater endmembers ranged from 5.76 μmol/L to 63.7 μmol/L, 0.23 μmol/L to 0.37 μmol/L and 8.02 μmol/L to 48.8 μmol/L, for DIN, DIP and DSi, respectively. The SGD-derived nutrient fluxes were calculated to be 0.14 × 10^5 mol/d to 1.51 × 10^5 mol/d for DIN, 5.55 × 10^2 mol/d to 8.74 × 10^2 mol/d for DIP and 0.19 × 10^5 mol/d to 1.16 × 10^5 mol/d for DSi, respectively.

4.3.2 *Budgets of DIN and DIP in the upper Kongsfjorden*

The Arctic region is less directly disturbed by human activities and is more sensitive to environmental changes. Global warming will lead to increased melting of glaciers and frozen soil in the Arctic region, causing SGD changes and their potential impacts on the offshore ecological environment and need to be studied urgently. Generally, river runoff, atmospheric deposition, etc., have long been recognized as major sources of nutrient in coastal areas (Berelson et al., 1998; Wang et al., 2018). The Arctic region is affected by global warming, we need to consider the im-

pact of nutrient transported by the melting of floating ice and glacier. In order to better evaluate the nutrient level of the Kongsfjorden, we established the DIN and DIP budgets in upper 10 m water by considering the impact of SGD (Fig. 5).

Riverine nutrient fluxes into the coastal area are regarded as a crucial source for bay ecosystems (Jickells, 1998). The nutrient fluxes delivered by the river were estimated by multiplying the river discharge by the concentrations of the nutrient in the river water endmember. The measured nutrient concentrations for DIN and DIP in the Bayelva River were 11.8 μmol/L and 0.33 μmol/L, resulting in the riverine DIN and DIP fluxes being 9.67×10^2 mol/d and 27 mol/d, respectively.

Due to the influence of global warming and the North Atlantic Current, a large area of floating ice and glacier melted during the sampling period, the melting of floating ice also transported a certain amount of nutrient. The floating ice area of Kongsfjorden is 1.05×10^7 m^2, and the nutrient concentrations in the floating ice meltwater were 0.53 μmol/L for DIN and 0.02 μmol/L for DIP (Zhu et al., 2016). The melting rate of the floating ice was 0.44 cm/d (Hop and Wiencke, 2019). The nutrient fluxes through the floating ice meltwater were estimated to be 2.46×10^2 mol/d and 9.22 mol/d for DIN and DIP, respectively. In addition, the DIN and DIP concentrations in glacier meltwater were 0.42 μmol/L and 0.02 μmol/L, respectively. Thus, DIN and DIP fluxes from the glacier meltwater were estimated to be 73.1 mol/d and 3.46 mol/d, respectively.

Another traditional source of nutrient is atmospheric deposition. Nutrient fluxes through atmospheric deposition were estimated by multiplying the area of the Kongsfjorfen with nutrient deposition rates. The average atmospheric deposition fluxes of DIN to the entire Arctic Ocean to be 3 650 kg/(hm^2·d) (in terms of N) (Stewart et al., 2014). The Kongsfjorden is adjacent to the Arctic Ocean, we substituted atmospheric deposition fluxes in the Arctic Ocean for those in the Kongsfjorden. Therefore, the DIN fluxes through atmospheric deposition in the Kongsfjorden were estimated to be 4.09×10^4 mol/d.

In general, mixing loss to the open sea and absorption by phytoplankton have been recognized as the main sinks of nutrients in coastal regions (Chen et al., 2020; Peng et al., 2021; Wang et al., 2014). The output fluxes through those processes are shown in Fig. 5.

In the process of glacier melting in summer, glacial meltwater has a significant impact on the growth of phytoplankton in the Kongsfjorden (Piquet et al., 2014). Seasonal changes in glacier melting have changed the distribution characteristics of phytoplankton, leading to changes in nutrient structure in Kongsfjorden. The primary productivity of Kongsfjorden in summer is 700 mg/(m·d) (in terms of C) (Kim et al., 2020), the nutrient fluxes through absorption by phytoplankton were estimated to be 1.30×10^6 mol/d and 4.45×10^4 mol/d, respectively.

The change of tide leads to the mixing of the inner bay water and open-sea water, which results in the loss of nutrient. The Arctic Ocean has been considered the main nutrient sink. Nutrient fluxes via mixing losses were calculated by the method adopted from Chen et al. (2018). In this study, the mean DIN and DIP concentrations in surface water were 6.81 μmol/L and 0.279 μmol/L, respectively, while DIN and DIP concentrations in open-sea endmember were 4.53 μmol/L and 0.205 μmol/L, respectively. So the fluxes of DIN and DIP through mixing loss were calculated to be $(1.60 \pm 0.34) \times 10^5$ mol/d and $(5.19 \pm 1.11) \times 10^3$ mol/d, respectively. In contrast to SGD, the nutrient fluxes through mixing losses correspond to the major portion of the SGD-derived nutrient fluxes.

The nutrient budgets in the Kongsfjorden indicated that SGD accounted for 24.5%–78.1% of DIN and 93.3%–95.7% of DIP input and we can see SGD was the dominant nutrient source for this fjord. Besides, riverine input contributed 0.5%–1.7% of DIN and 3.0%–4.6% of DIP. Therefore, nutrient through river was negligible compared to those from SGD. In addition, we also found that the total sources were lower than the sinks, indicating that some sources in the system were not considered, such as the degradation of organic matter, which provided the material basis for nutrient.

4.4 *Comparison of SGD cases around the Arctic Ocean*

The scale of SGD studies varies greatly, most of those have focused on fluxes and related solutes in some regions, such as beaches, bays or estuaries (Dimova and Burnett, 2011; Knee and Paytan, 2011; Santos et al., 2021; Taniguchi et al., 2003). Some studies attempted to quantify SGD from large-scale sea areas and

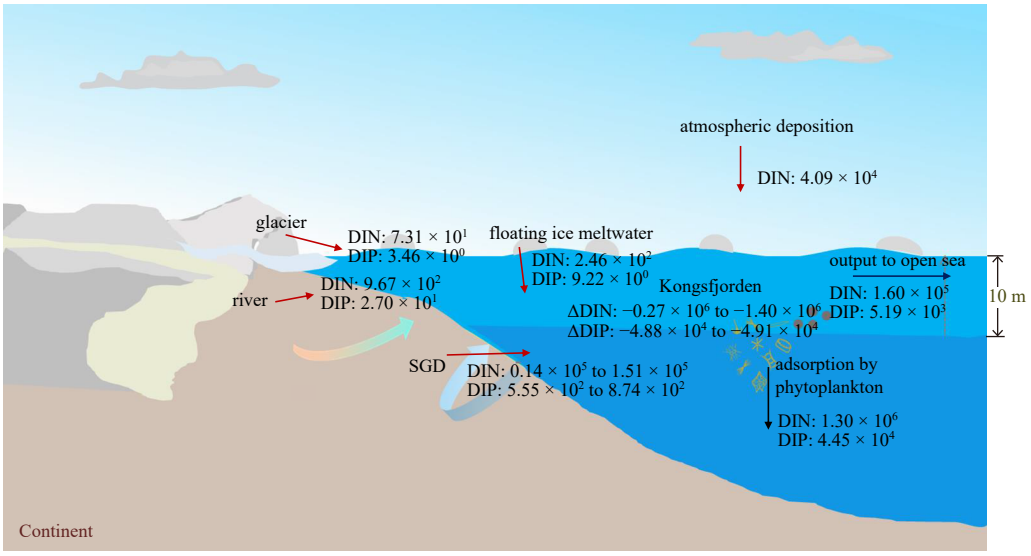

Fig. 5. Schematic diagram for DIN and DIP budgets (all in mol/d) in the upper Kongsfjorden during our sampling period [some data from Piquet et al. (2014), Stewart et al. (2014), Zhu et al. (2016), Chen et al. (2018), Hop and Wiencke (2019), Kim et al. (2020)].

the model of global SGD to the ocean has become a research hotspot in recent years (Moore, 2010; Kwon et al., 2014; Santos et al., 2021). These large-scale studies basically focused on the North Atlantic basin and other easily accessible ocean basins, while the most extensive studies also ignored the Arctic Ocean in their calculations (Charette et al., 2013; Kwon et al., 2014). Despite the Arctic covering an area of about 3×10^{13} m^2, the research on SGD has been only limited.

In recent years, studies on SGD flux in polar regions have been increasing. Some studies were based on coastlines, Frederick and Buffett (2015) indicated that SGD flux in the Mackenzie River Mouth was 0.16–0.38 m^3/(m·d). Walvoord and Striegl (2007) found that SGD flux in the Yukon River Basin accounted for 31%–38% of the local river. For an all-around comparison, we summarized all study cases with specific SGD flux in the Arctic region to date (Fig. 6). According to the distribution of SGD cases, we found that most of those were concentrated in Alaska, and there were fewer studies in other places (Fig. 6a). In the Arctic region, the SGD rate has an extensive range from 0.01 cm/d to 187 cm/d. In the present study, the SGD rate in the Kongsfjorden was inside this wide range, and ever larger than the median value. But the value is much smaller compared to that in the Kasitsna Bay [(187 ± 67) cm/d], mainly on account of high tidal pumping effects, precipitation and topographic undulation (Lecher, 2015). Compared with the Cambridge Fjord of the same type, the SGD rate in Kongsfjord is much larger than that estimated in 1984, which may be mainly because of the global warming in the last 20 years, and then indirectly led to the increase of SGD (Hay, 1984). Furthermore, the SGD rate shows a slightly increasing trend with the increase of years, which may be due to the enhanced flow as groundwater flow paths are activated between land and coastal waters as a result of the warming climate and accelerated permafrost thawing (Duan et al., 2017; Guimond et al., 2022; Jacques and Sauchyn, 2009; Walvoord et al., 2019). It is worth noting that climate warming leads to rising sea levels, which have the potential to alter land-sea hydraulic gradients, leading to complex interactions that may control future coastal groundwater discharge dynamics along the Arctic coastline (Guimond et al., 2022). Studies have shown that coastal groundwater discharge will increase by 58% by 2100, due to the formation of suprapermafrost aquifers that enhance the ability to deliver fresh water to coastal areas (Guimond et al., 2022; Michael et al., 2005).

The surface water of the Arctic Ocean contains a large amount of fresh water, changes in the inventory of fresh water in the Arctic Ocean have been particularly dramatic in recent decades, with important implications for global climate (Bridgestock et al., 2021b; Carmack et al., 2016; Rabe et al., 2014). Riverine input is the crucial source of fresh water in the Arctic Ocean, the flux was 4 200

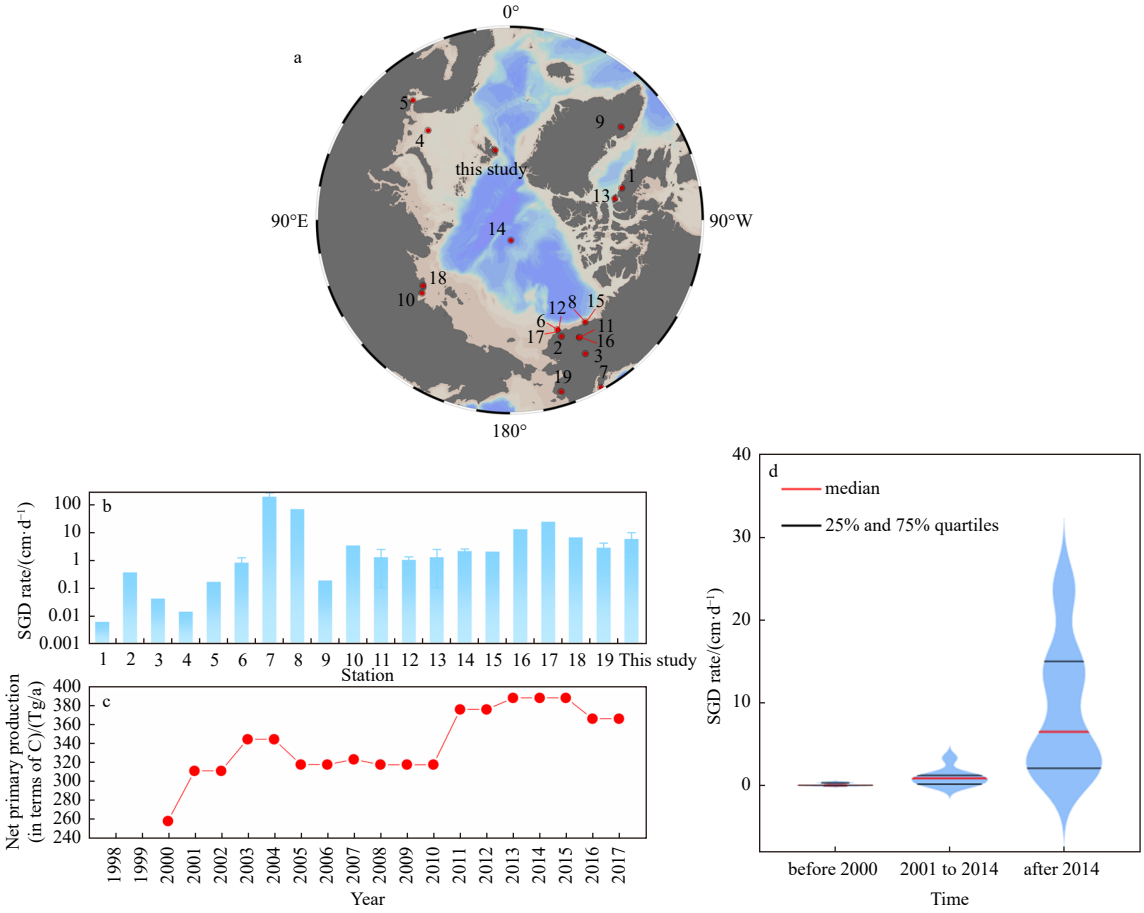

Fig. 6. Locations of SGD flux study cases, as viewed from the geographic North Pole (a); distribution of SGD rates (cm/d) for each study site in the Arctic Ocean, the numbers correspond to the study cases in a (b); the trend of net primary production in the Arctic Ocean from 2000 to 2017 that modified from Lewis et al. (2020) (c). The distribution of SGD rates (cm/d) in the Arctic Ocean from 1983 to 2017 (d). The SGD rate data from Connolly et al. (2020), Whalen and Cornwell (1985), Dabrowski et al. (2020), Deming et al. (1992), Dimova et al. (2015), Dzyuba and Zektser (2013), Hay (1984), Lecher et al. (2016a), Lecher (2017), Linhoff et al. (2017), Neilson et al. (2018), Wales et al. (2020), Whalen and Charkin (1985).

± 420 km^3/yr, which contributes to 11% of the global rivers (Haine et al., 2015; Rosén et al., 2015). The distribution of fresh water within the Arctic Ocean is further controlled by seasonal sea ice melting and changes in wind-driven circulation (Morison et al., 2012; Rosén et al., 2015). However, previous studies only focused on the importance of riverine input on fresh water supply in the Arctic Ocean, but usually overlooked the impact of coastal groundwater input. With global warming, rising sea levels and accelerated thawing of permafrost, the SGD would act as an increasing role on hydrological and nutrient cycles in the Arctic Ocean.

4.5 *Eco-Environmental impacts of SGD-derived nutrient in the Kongsfjorden*

Significant increases in N and P loads entering the bay can lead to an enhancement of phytoplankton biomass or ecosystem damage, such as dissolved oxygen consumption (McCoy et al., 2011), red tide (Lee et al., 2010; Luo and Jiao, 2016) and eutrophication (Hwang et al., 2005), thereby affecting global nutrient cycling (Glibert et al., 2008; Santos et al., 2021; Slomp and Van Cappellen, 2004). In the Kongsfjorden, we observed a relatively higher NIN/DIP molar ratio varied from 24.6 to 173 (average value: 98.8) in coastal groundwater than that in surface water and river water, which were 67.1 and 36, respectively (Fig. 7). Since the NIN/DIP molar ratio is often used to assess potential constraints in primary production, high NIN/DIP molar ratios in groundwater may force primary production conditions from N limitation to P limitation and affect microalgae community composition in the coastal areas (Lee et al., 2010; Su et al., 2011). The input of groundwater with a high NIN/DIP molar ratio along the coastal zones of the Kongsfjord may modify the nutrient structures and then influence the marine ecosystem. In addition, the dominant picophytoplankton in the Kongsfjorden was *cryptophyta/cyanobacteria* and glacial meltwater had a significant impact on the growth of this phytoplankton in the Kongsfjorden (Piquet et al., 2014). In late spring, the meltwater input caused the stratification of surface waters in the fjord. Therefore, a large amount of SGD input with a high NIN/DIP molar ratio has the potential to increase the biomass and then change community structure of phytoplankton in the fjord water, thus it is needed to be considered.

Rising temperatures in the Arctic Ocean have led to glacier reducing, permafrost melting and river flows increasing, which together alter the nutrient and carbon cycles on the vast Arctic continental shelf (Kipp et al., 2018). In the Arctic Ocean, net primary productivity is controlled by a complex interplay of light and nutrient provided by upwelling and lateral inflow from adjacent oceans and land (Terhaar et al., 2021). The input of terrigenous nutrient is a crucial process affecting the future evolution of net primary productivity in the Arctic Ocean. Up to now, we usually ignored the role of SGD-derived nutrient on the Arctic net primary productivity. Due to the unique geography of the Arctic Ocean, SGD would be a greater impact on marine net primary productivity than other ocean regions (Lewis et al., 2020; Terhaar et al., 2021). We summarized the data on Arctic Ocean net primary productivity from 2000 to 2017 and found a significant increase (approximately 42%) of net primary productivity in the Arctic Ocean. The increase in net primary productivity during 1998–2008 was due to widespread sea ice loss, which resulted in an increase in open water and a longer growing season for phytoplankton. But the subsequent increase in net primary production is mainly due to an increase in phytoplankton biomass, which must be sustained by providing more extra nutrient to the system (Arrigo and van Dijken, 2011; Lewis et al., 2020; Zhang et al., 2010). Overall, the trend of increasing net primary production in the Arctic Ocean showed a very similar trend to the increasing SGD rate sorted by years around the Arctic Ocean (Fig. 6), suggesting that SGD has the potential to enhance the net primary production in the Arctic Ocean. To the extent that the increase in nutrient supplies is driven by processes associated with climate change, such as SGD and glacial meltwater, and the Arctic Ocean may support higher nutrient level production in the future.

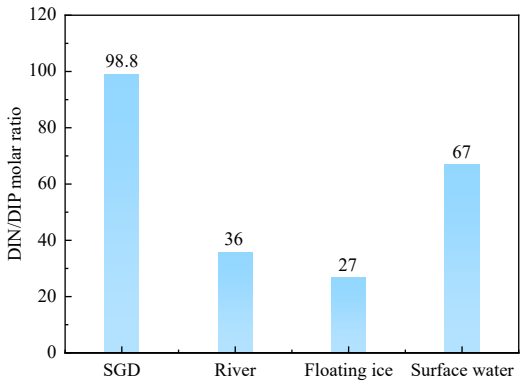

Fig. 7. The DIN/DIP molar ratios in SGD, river water, floating ice and surface seawater in the Kongsfjorden.

5 Conclusions

In the high latitude bay of the Kongdfjorden, we used a mass balance model based on radium isotopes, to assess the environmental impact of SGD under the influence of global warming. SGD and it derived nutrient fluxes into the Kongsfjorden were quantified for the first time. SGD flux was calculated to be (2.37 ± 0.70) × 10^6 m^3/d, which was 29 times the flow of the local river. The estimated nutrient fluxes derived by SGD were 0.14 × 10^5 mol/d to 1.51 × 10^5 mol/d for DIN, 5.55 × 10^2 mol/d to 8.74 × 10^2 mol/d for DIP and 0.19 × 10^5 mol/d to 1.16 × 10^5 mol/d for DSi, respectively, which were three orders of magnitude higher than the riverine inputs. The high NIN/DIP molar ratio by SGD (98.8) was significantly higher than that in surface water (67.1). Such high ratios can heavily impact the ecosystem by changing the biomass and community structure of phytoplankton following accelerating global warming. The form of SGD in the Arctic is unique, with global warming causing permafrost to melt faster, seep down into aquifers and discharged into the coastal region as groundwater. SGD in the Arctic is discharged in a similar proportion to river water, which means that in a rapidly changing climate, SGD may play a significant role in transporting solutes to the Arctic Ocean, which may be an important reason for the increase in net primary productivity in the Arctic Ocean in recent years.

Acknowledgements

We greatly appreciate the staff at Kingsfjorden for their assistance during the sampling period.

References

Arrigo K R, van Dijken G L. 2011. Secular trends in Arctic Ocean net primary production. Journal of Geophysical Research: Oceans, 116(C9): C09011, doi: 10.1029/2011JC007151

Baléo J N, Humeau P, Le Cloirec P. 2001. Numerical and experimental hydrodynamic studies of a lagoon pilot. Water Research, 35(9): 2268–2276, doi: 10.1016/S0043-1354(00)00502-9

Berelson W M, Heggie D, Longmore A, et al. 1998. Benthic nutrient

recycling in Port Phillip Bay, Australia. Estuarine, Coastal and Shelf Science, 46(6): 917–934,doi: 10.1006/ecss.1998.0328
Bridgestock L, Nathan J, Hsieh Y T, et al. 2021a. Assessing the utility of barium isotopes to trace Eurasian riverine freshwater inputs to the Arctic Ocean. Marine Chemistry, 236: 104029, doi: 10.1016/j.marchem.2021.104029
Bridgestock L, Nathan J, Paver R, et al. 2021b. Estuarine processes modify the isotope composition of dissolved riverine barium fluxes to the ocean. Chemical Geology, 579: 120340, doi: 10.1016/j.chemgeo.2021.120340
Bullock E J, Kipp L, Moore W, et al. 2022. Radium inputs into the Arctic Ocean from rivers: A basin-wide estimate. Journal of Geophysical Research: Oceans, 127(9): e2022JC018964, doi: 10.1029/2022JC018964
Burnett W C, Bokuniewicz H, Huettel M, et al. 2003. Groundwater and pore water inputs to the coastal zone. Biogeochemistry, 66(1): 3–33, doi: 10.1023/B:BIOG.0000006066.21240.53
Burnett W C, Peterson R, Moore W S, et al. 2008. Radon and radium isotopes as tracers of submarine groundwater discharge-Results from the Ubatuba, Brazil SGD assessment intercomparison. Estuarine, Coastal and Shelf Science, 76(3): 501–511, doi: 10.1016/j.ecss.2007.07.027
Carmack E C, Yamamoto-Kawai M, Haine T W N, et al. 2016. Freshwater and its role in the Arctic Marine System: Sources, disposition, storage, export, and physical and biogeochemical consequences in the Arctic and global oceans. Journal of Geophysical Research: Biogeosciences, 121(3): 675–717, doi: 10.1002/2015JG003140
Cerdà-Domènech M, Rodellas V, Folch A, et al. 2017. Constraining the temporal variations of Ra isotopes and Rn in the groundwater end-member: Implications for derived SGD estimates. Science of the Total Environment, 595: 849–857, doi: 10.1016/j.scitotenv.2017.03.005
Charette M A, Breier C F, Henderson P B, et al. 2013. Radium-based estimates of cesium isotope transport and total direct ocean discharges from the Fukushima Nuclear Power Plant accident. Biogeosciences, 10(3): 2159–2167, doi: 10.5194/bg-10-2159-2013
Charkin A N, Dudarev O V, Semiletov I P, et al. 2011. Seasonal and interannual variability of sedimentation and organic matter distribution in the Buor-Khaya Gulf: the primary recipient of input from Lena River and coastal erosion in the southeast Laptev Sea. Biogeosciences, 8(9): 2581–2594, doi: 10.5194/bg-8-2581-2011
Charkin A N, van der Loeff M R, Shakhova N E, et al. 2017. Discovery and characterization of submarine groundwater discharge in the Siberian Arctic seas: a case study in the Buor-Khaya Gulf, Laptev Sea. The Cryosphere, 11(5): 2305–2327, doi: 10.5194/tc-11-2305-2017
Chen Xiaogang, Cukrov N, Santos I R, et al., 2020. Karstic submarine groundwater discharge into the Mediterranean: Radon-based nutrient fluxes in an anchialine cave and a basin-wide upscaling. Geochimica et Cosmochimica Acta, 268: 467–484, doi: 10.1016/j.gca.2019.08.019
Chen Meilian, Kim J H, Nam S I, et al. 2016. Production of fluorescent dissolved organic matter in Arctic Ocean sediments. Scientific Reports, 6(1): 39213, doi: 10.1038/srep39213
Chen Xiaogang, Lao Yanling, Wang Jinlong, et al. 2018. Submarine groundwater-borne nutrients in a tropical bay (Maowei Sea, China) and their impacts on the oyster aquaculture. Geochemistry, Geophysics, Geosystems, 19(3): 932–951,doi: 10.1002/2017GC007330
Cho H M, Kim G. 2017. Large temporal changes in contributions of groundwater-borne nutrients to coastal waters off a volcanic island. Ocean Science Journal, 52(3): 337–344, doi: 10.1007/s12601-017-0033-4
Collins M, Knutti R, Arblaster J, et al. 2013. Long-term climate change: projections, commitments and irreversibility. In: Climate Change 2013—The Physical Science Basis: Contribution of Working Group I to the fifth Assessment Report of the Intergovernmental Panel on Climate Change. New York, USA: Cambridge University Press, 1029–1136
Connolly C T, Cardenas M B, Burkart G A, et al. 2020. Groundwater as a major source of dissolved organic matter to Arctic coastal waters. Nature Communications, 11(1): 1479, doi: 10.1038/s41467-020-15250-8
Dabrowski J S, Charette M A, Mann P J, et al. 2020. Using radon to quantify groundwater discharge and methane fluxes to a shallow, tundra lake on the Yukon-Kuskokwim Delta, Alaska. Biogeochemistry, 148(1): 69–89, doi: 10.1007/s10533-020-00647-w
Deming D, Sass J H, Lachenbruch A H, et al. 1992. Heat flow and subsurface temperature as evidence for basin-scale ground-water flow, North Slope of Alaska. GSA Bulletin, 104(5): 528–542, doi: 10.1130/0016-7606(1992)104<0528:HFASTA>2.3.CO;2
Dimova N T, Burnett W C. 2011. Evaluation of groundwater discharge into small lakes based on the temporal distribution of radon-222. Limnology and Oceanography, 56(2): 486–494, doi: 10.4319/lo.2011.56.2.0486
Dimova N T, Paytan A, Kessler J D, et al. 2015. Current magnitude and mechanisms of groundwater discharge in the Arctic: Case study from Alaska. Environmental Science & Technology, 49(20): 12036–12043, doi: 10.1021/acs.est.5b02215
Duan Liangliang, Man Xiuling, Kurylyk B L, et al. 2017. Increasing winter baseflow in response to permafrost thaw and precipitation regime shifts in northeastern China. Water, 9(1): 25, doi: 10.3390/w9010025
Dzyuba A V, Zektser I S. 2013. Variations in submarine groundwater runoff as a possible cause of decomposition of marine methane-hydrates in the Arctic. Water Resources, 40(1): 74–83, doi: 10.1134/S009780781301003x
Frederick J M, Buffett B A. 2015. Effects of submarine groundwater discharge on the present-day extent of relict submarine permafrost and gas hydrate stability on the Beaufort Sea continental shelf. Journal of Geophysical Research: Earth Surface, 120(3): 417–432, doi: 10.1002/2014JF003349
Garcia-Orellana J, Rodellas V, Tamborski J, et al. 2021. Radium isotopes as submarine groundwater discharge (SGD) tracers: Review and recommendations. Earth-Science Reviews, 220: 103681, doi: 10.1016/j.earscirev.2021.103681
Geyer W R, Morris J T, Prahl F G, et al. 2000. Interaction between physical processes and ecosystem structure: A comparative approach. In: Hobbie J, ed. Estuarine Science: A Synthetic Approach to Research and Practice. Washington, DC: Island Press, 177–206
Glibert P M, Mayorga E, Seitzinger S. 2008. Prorocentrum minimum tracks anthropogenic nitrogen and phosphorus inputs on a global basis: application of spatially explicit nutrient export models. Harmful Algae, 8(1): 33–38, doi: 10.1016/j.hal.2008.08.023
Guimond J A, Mohammed A A, Walvoord M A, et al. 2022. Sea-level rise and warming mediate coastal groundwater discharge in the Arctic. Environmental Research Letters, 17(4): 045027, doi: 10.1088/1748-9326/ac6085
Haine T W N, Curry B, Gerdes R, et al. 2015. Arctic freshwater export: Status, mechanisms, and prospects. Global and Planetary Change, 125: 13–35, doi: 10.1016/j.gloplacha.2014.11.013
Haldorsen S, Heim M. 1999. An Arctic groundwater system and its dependence upon climatic change: an example from Svalbard. Permafrost and Periglacial Processes, 10(2): 137–149, doi: 10.1002/(SICI)1099-1530(199904/06)10:2<137::AID-PPP316>3.0.CO;2-#
Hay A E. 1984. Remote acoustic imaging of the plume from a submarine spring in an Arctic fjord. Science, 225(4667): 1154–1156, doi: 10.1126/science.225.4667.1154
Hodson A J, Nowak A, Redeker K R, et al. 2019. Seasonal dynamics of methane and carbon dioxide evasion from an open system pingo: Lagoon pingo, Svalbard. Frontiers in Earth Science, 7: 30, doi: 10.3389/feart.2019.00030
Hop H, Wiencke C. 2019. The ecosystem of Kongsfjorden, Svalbard. In: The Ecosystem of Kongsfjorden, Svalbard. Cham: Springer, 1–20
Hwang D W, Kim G, Lee W C, et al. 2010. The role of submarine groundwater discharge (SGD) in nutrient budgets of Gamak Bay, a shellfish farming bay, in Korea. Journal of Sea Research, 64(3): 224–230, doi: 10.1016/j.seares.2010.02.006

Hwang D W, Kim G, Lee Y W, et al. 2005. Estimating submarine inputs of groundwater and nutrients to a coastal bay using radium isotopes. Marine Chemistry, 96(1–2): 61–71, doi: 10.1016/j.marchem.2004.11.002

Jacques J M St, Sauchyn D J. 2009. Increasing winter baseflow and mean annual streamflow from possible permafrost thawing in the Northwest Territories, Canada. Geophysical Research Letters, 36(1): L01401, doi: 10.1029/2008GL035822

Jickells T D. 1998. Nutrient biogeochemistry of the coastal zone. Science, 281(5374): 217–222, doi: 10.1126/science.281.5374.217

Kim B K, Joo H M, Jung J, et al. 2020. *In situ* rates of carbon and nitrogen uptake by phytoplankton and the contribution of picophytoplankton in Kongsfjorden, Svalbard. Water, 12(10): 2903, doi: 10.3390/w12102903

Kim G, Kim J S, Hwang D W. 2011. Submarine groundwater discharge from oceanic islands standing in oligotrophic oceans: Implications for global biological production and organic carbon fluxes. Limnology and Oceanography, 56(2): 673–682, doi: 10.4319/lo.2011.56.2.0673

Kim J H, Ryu J S, Hong W L, et al. 2022. Assessing the impact of freshwater discharge on the fluid chemistry in the Svalbard fjords. Science of the Total Environment, 835: 155516, doi: 10.1016/j.scitotenv.2022.155516

Kim G, Ryu J W, Yang H S, et al. 2005. Submarine groundwater discharge (SGD) into the Yellow Sea revealed by ^{228}Ra and ^{226}Ra isotopes: Implications for global silicate fluxes. Earth and Planetary Science Letters, 237(1–2): 156–166, doi: 10.1016/j.epsl.2005.06.011

Kipp L E, Charette M A, Moore W S, et al. 2018. Increased fluxes of shelf-derived materials to the central Arctic Ocean. Science Advances, 4(1): eaao1302, doi: 10.1126/sciadv.aao1302

Knee K L, Paytan A. 2011. Submarine groundwater discharge: a source of nutrients, metals, and pollutants to the coastal ocean. In: Wolanski E, McLusky D, eds. Treatise on Estuarine and Coastal Science. Amsterdam: Academic Press, 4: 205–233

Kuliński K, Kędra M, Legeżyńska J, et al. 2014. Particulate organic matter sinks and sources in high Arctic fjord. Journal of Marine Systems, 139: 27–37, doi: 10.1016/j.jmarsys.2014.04.018

Kwon E Y, Kim G, Primeau F, et al. 2014. Global estimate of submarine groundwater discharge based on an observationally constrained radium isotope model. Geophysical Research Letters, 41(23): 8438–8444, doi: 10.1002/2014GL061574

Lecher A L. 2015. From the land to the sea: Impacts of submarine groundwater discharge on the coastal ocean of California and Alaska [dissertation]. Santa Cruz: University of California

Lecher A L. 2017. Groundwater discharge in the Arctic: A review of studies and implications for biogeochemistry. Hydrology, 4(3): 41, doi: 10.3390/hydrology4030041

Lecher A L, Chien C T, Paytan A. 2016a. Submarine groundwater discharge as a source of nutrients to the North Pacific and Arctic coastal ocean. Marine Chemistry, 186: 167–177, doi: 10.1016/j.marchem.2016.09.008

Lecher A L, Kessler J, Sparrow K, et al. 2016b. Methane transport through submarine groundwater discharge to the North Pacific and Arctic Ocean at two Alaskan sites. Limnology and Oceanography, 61(S1): S344–S355, doi: 10.1002/lno.10118

Lee Y W, Kim G, Lim W A, et al. 2010. A relationship between submarine groundwater borne nutrients traced by Ra isotopes and the intensity of dinoflagellate red-tides occurring in the southern sea of Korea. Limnology and Oceanography, 55(1): 1–10, doi: 10.4319/lo.2010.55.1.0001

Lewis K M, Van Dijken G L, Arrigo K R. 2020. Changes in phytoplankton concentration now drive increased Arctic Ocean primary production. Science, 369(6500): 198–202, doi: 10.1126/science.aay8380

Linhoff B S, Charette M A, Nienow P W, et al. 2017. Utility of ^{222}Rn as a passive tracer of subglacial distributed system drainage. Earth and Planetary Science Letters, 462: 180–188, doi: 10.1016/j.epsl.2016.12.039

Linhoff B S, Charette M A, Wadham J. 2020. Rapid mineral surface weathering beneath the Greenland Ice Sheet shown by radium and uranium isotopes. Chemical Geology, 547: 119663, doi: 10.1016/j.chemgeo.2020.119663

Liu Jian'an, Du Jinzhou, Yi Lixin. 2017. Ra tracer-based study of submarine groundwater discharge and associated nutrient fluxes into the Bohai Sea, China: A highly human-affected marginal sea. Journal of Geophysical Research: Oceans, 122(11): 8646–8660, doi: 10.1002/2017jc013095

Liu Jian'an, Du Jinzhou, Yu Xueqing. 2021. Submarine groundwater discharge enhances primary productivity in the Yellow Sea, China: Insight from the separation of fresh and recirculated components. Geoscience Frontiers, 12(6): 101204, doi: 10.1016/j.gsf.2021.101204

Liu Sumei, Hong G H, Zhang Jing, et al. 2009. Nutrient budgets for large Chinese estuaries. Biogeosciences, 6(10): 2245–2263, doi: 10.5194/bg-6-2245-2009

Liu Jian'an, Liu Dongyan, Du Jinzhou. 2022. Radium-traced nutrient outwelling from the Subei Shoal to the Yellow Sea: Fluxes and environmental implication. Acta Oceanologica Sinica, 41(6): 12–21, doi: 10.1007/s13131-021-1930-z

Luo Xin, Jiao Jiu Jimmy. 2016. Submarine groundwater discharge and nutrient loadings in Tolo Harbor, Hong Kong using multiple geotracer-based models, and their implications of red tide outbreaks. Water Research, 102: 11–31, doi: 10.1016/j.watres.2016.06.017

Luo Xin, Jiao Jiu Jimmy, Moore W S, et al. 2014. Submarine groundwater discharge estimation in an urbanized embayment in Hong Kong via short-lived radium isotopes and its implication of nutrient loadings and primary production. Marine Pollution Bulletin, 82(1–2): 144–154, doi: 10.1016/j.marpolbul.2014.03.005

McCoy C, Viso R, Peterson R N, et al. 2011. Radon as an indicator of limited cross-shelf mixing of submarine groundwater discharge along an open ocean beach in the South Atlantic Bight during observed hypoxia. Continental Shelf Research, 31(12): 1306–1317, doi: 10.1016/j.csr.2011.05.009

McGovern M, Warner N A, Borga K, et al. 2022. Is Glacial Meltwater a Secondary Source of Legacy Contaminants to Arctic Coastal Food Webs?. Environmental Science and Technology, 56(10): 6337–6348, doi: 10.1021/acs.est.1c07062

Michael H A, Mulligan A E, Harvey C F. 2005. Seasonal oscillations in water exchange between aquifers and the coastal ocean. Nature, 436(7054): 1145–1148, doi: 10.1038/nature03935

Moore W S. 1996. Large groundwater inputs to coastal waters revealed by ^{226}Ra enrichments. Nature, 380(6575): 612–614, doi: 10.1038/380612a0

Moore W S. 2010. The effect of submarine groundwater discharge on the ocean. Annual Review of Marine Science, 2(1): 59–88, doi: 10.1146/annurev-marine-120308-081019

Moore W S, Arnold R. 1996. Measurement of ^{223}Ra and ^{224}Ra in coastal waters using a delayed coincidence counter. Journal of Geophysical Research: Oceans, 101 (C1): 1321–1329, doi: 10.1029/95JC03139

Moore W S, Blanton J O, Joye S B. 2006. Estimates of flushing times, submarine groundwater discharge, and nutrient fluxes to Okatee Estuary, South Carolina. Journal of Geophysical Research: Oceans, 111(C9): C09006, doi: 10.1029/2005JC003041

Morison J, Kwok R, Peralta-Ferriz C, et al. 2012. Changing Arctic Ocean freshwater pathways. Nature, 481(7379): 66–70, doi: 10.1038/nature10705

Neilson B T, Cardenas M B, O'Connor M T, et al. 2018. Groundwater flow and exchange across the land surface explain carbon export patterns in continuous permafrost watersheds. Geophysical Research Letters, 45(15): 7596–7605, doi: 10.1029/2018gl078140

Oehler T, Eiche E, Putra D, et al. 2018. Seasonal variability of land-ocean groundwater nutrient fluxes from a tropical karstic region (southern Java, Indonesia). Journal of Hydrology, 565: 662–671, doi: 10.1016/j.jhydrol.2018.08.077

Olichwer T, Tarka R, Modelska M. 2013. Chemical composition of groundwaters in the Hornsund region, southern Spitsbergen. Hydrology Research, 44(1): 117–130, doi: 10.2166/nh.2012.075

Peng Tong, Zhu Zhuoyi, Du Jinzhou, et al. 2021. Effects of nutrient-rich submarine groundwater discharge on marine aquaculture: A case in Lianjiang, East China Sea. Science of the Total Environment, 786: 147388, doi: 10.1016/j.scitotenv.2021.147388

Peral M, Austin W E N, Noormets R. 2022. Identification of Atlantic water inflow on the north Svalbard shelf during the Holocene. Journal of Quaternary Science, 37(1): 86–99, doi: 10.1002/jqs.3374

Peterson B J, Holmes R M, McClelland J W, et al. 2002. Increasing river discharge to the Arctic Ocean. Science, 298(5601): 2171–2173, doi: 10.1126/science.1077445

Piquet A M T, Van de Poll W H, Visser R J W, et al. 2014. Springtime phytoplankton dynamics in the Arctic Krossfjorden and Kongsfjorden (Spitsbergen) as a function of glacier proximity. Biogeosciences, 11(8): 2263–2279, doi: 10.5194/bgd-10-15519-2013

Polyakov I V, Walsh J E, Kwok R. 2012. Recent changes of Arctic multiyear sea ice coverage and the likely causes. Bulletin of the American Meteorological Society, 93(2): 145–151, doi: 10.1175/BAMS-D-11-00070.1

Rabe B, Karcher M, Kauker F, et al. 2014. Arctic Ocean basin liquid freshwater storage trend 1992–2012. Geophysical Research Letters, 41(3): 961–968, doi: 10.1002/2013GL058121

Rodellas V, Garcia-Orellana J, Masqué P, et al. 2015. Submarine groundwater discharge as a major source of nutrients to the Mediterranean Sea. Proceedings of the National Academy of Sciences of the United States of America, 112(13): 3926–3930, doi: 10.1073/pnas.1419049112

Rosén P O, Andersson P S, Alling V, et al. 2015. Ice export from the Laptev and East Siberian Sea derived from $\delta^{18}O$ values. Journal of Geophysical Research: Oceans, 120(9): 5997–6007, doi: 10.1002/2015JC010866

Sadat-Noori M, Santos I R, Sanders C J, et al. 2015. Groundwater discharge into an estuary using spatially distributed radon time series and radium isotopes. Journal of Hydrology, 528: 703–719, doi: 10.1016/j.jhydrol.2015.06.056

Sanford L P, Boicourt W C, Rives S R. 1992. Model for estimating tidal flushing of small embayments. Journal of Waterway, Port, Coastal, and Ocean Engineering, 118(6): 635–654, doi: 10.1061/(ASCE)0733-950X(1992)118:6(635)

Santos I R, Chen Xiaogang, Lecher A L, et al. 2021. Submarine groundwater discharge impacts on coastal nutrient biogeochemistry. Nature Reviews Earth & Environment, 2(5): 307–323, doi: 10.1038/s43017-021-00152-0

Santos I R, Eyre B D, Huettel M. 2012. The driving forces of porewater and groundwater flow in permeable coastal sediments: A review. Estuarine, Coastal and Shelf Science, 98: 1–15, doi: 10.1016/j.ecss.2011.10.024

Semenov P, Portnov A, Krylov A, et al. 2020. Geochemical evidence for seabed fluid flow linked to the subsea permafrost outer border in the South Kara Sea. Geochemistry, 80(3): 125509, doi: 10.1016/j.chemer.2019.04.005

Sinha R K, Krishnan K P, Hatha A A, et al. 2017. Diversity of retrievable heterotrophic bacteria in Kongsfjorden, an Arctic fjord. Brazilian Journal of Microbiology, 48(1): 51–61, doi: 10.1016/j.bjm.2016.09.011

Slomp C P, Van Cappellen P. 2004. Nutrient inputs to the coastal ocean through submarine groundwater discharge: controls and potential impact. Journal of Hydrology, 295(1–4): 64–86, doi: 10.1016/j.jhydrol.2004.02.018

Smith L C, Sheng Yongwei, MacDonald G M. 2007. A first pan-Arctic assessment of the influence of glaciation, permafrost, topography and peatlands on northern hemisphere lake distribution. Permafrost and Periglacial Processes, 18(2): 201–208, doi: 10.1002/ppp.581

Stewart K J, Grogan P, Coxson D S, et al. 2014. Topography as a key factor driving atmospheric nitrogen exchanges in Arctic terrestrial ecosystems. Soil Biology and Biochemistry, 70: 96–112, doi: 10.1016/j.soilbio.2013.12.005

Su Ni, Du Jinzhou, Moore W S, et al. 2011. An examination of groundwater discharge and the associated nutrient fluxes into the estuaries of eastern Hainan Island, China using ^{226}Ra. Science of the Total Environment, 409(19): 3909–3918, doi: 10.1016/j.scitotenv.2011.06.017

Svendsen H, Beszczynska-Møller A, Hagen J O, et al. 2002. The physical environment of Kongsfjorden– Krossfjorden, an Arctic fjord system in Svalbard. Polar Research, 21(1): 133–166, doi: 10.1016/j.ecss.2006.07.022

Swarzenski P W. 2007. U/Th series radionuclides as coastal groundwater tracers. Chemical Reviews, 107(2): 663–674, doi: 10.1021/cr0503761

Taniguchi M, Burnett W C, Smith C F, et al. 2003. Spatial and temporal distributions of submarine groundwater discharge rates obtained from various types of seepage meters at a site in the Northeastern Gulf of Mexico. Biogeochemistry, 66(1–2): 35–53, doi: 10.1023/B:BIOG.0000006090.25949.8d

Terhaar J, Lauerwald R, Regnier P, et al. 2021. Around one third of current Arctic Ocean primary production sustained by rivers and coastal erosion. Nature Communications, 12(1): 169, doi: 10.1038/s41467-020-20470-z

Torsvik T, Albretsen J, Sundfjord A, et al. 2019. Impact of tidewater glacier retreat on the fjord system: Modeling present and future circulation in Kongsfjorden, Svalbard. Estuarine, Coastal and Shelf Science, 220: 152–165, doi: 10.1016/j.ecss.2019.02.005

Vonk J E, Sánchez-García L, Van Dongen B E, et al. 2012. Activation of old carbon by erosion of coastal and subsea permafrost in Arctic Siberia. Nature, 489(7414): 137–140, doi: 10.1038/nature11392

Wales N A, Gomez-Velez J D, Newman B D, et al. 2020. Understanding the relative importance of vertical and horizontal flow in ice-wedge polygons. Hydrology and Earth System Sciences, 24(3): 1109–1129, doi: 10.5194/hess-24-1109-2020

Walvoord M A, Striegl R G. 2007. Increased groundwater to stream discharge from permafrost thawing in the Yukon River basin: Potential impacts on lateral export of carbon and nitrogen. Geophysical Research Letters, 34(12), doi: 10.1029/2007GL030216

Walvoord M A, Voss C I, Ebel B A, et al. 2019. Development of perennial thaw zones in boreal hillslopes enhances potential mobilization of permafrost carbon. Environmental Research Letters, 14(1): 015003, doi: 10.1088/1748-9326/aaf0cc

Wang Xilong, Du Jinzhou, Ji Tao, et al. 2014. An estimation of nutrient fluxes via submarine groundwater discharge into the Sanggou Bay-A typical multi-species culture ecosystem in China. Marine Chemistry, 167: 113–122, doi: 10.1016/j.marchem.2014.07.002

Wang Xuejing, Li Hailong, Yang Jinzhong, et al. 2017. Nutrient inputs through submarine groundwater discharge in an embayment: A radon investigation in Daya Bay, China. Journal of Hydrology, 551: 784–792, doi: 10.1016/j.jhydrol.2017.02.036

Wang Xuejing, Li Hailong, Zheng Chunmiao, et al. 2018. Submarine groundwater discharge as an important nutrient source influencing nutrient structure in coastal water of Daya Bay, China. Geochimica et Cosmochimica Acta, 225: 52–65, doi: 10.1016/j.gca.2018.01.029

Whalen S C, Cornwell J C. 1985. Nitrogen, phosphorus, and organic carbon cycling in an Arctic Lake. Canadian Journal of Fisheries and Aquatic Sciences, 42(4): 797–808, doi: 10.1139/f85-102

Yang Yichao, Ren Jingling, Zhu Zhuoyi. 2022. Distributions and influencing factors of dissolved manganese in Kongsfjorden and Ny-Ålesund, Svalbard. ACS Earth and Space Chemistry, 6(5): 1259–1268, doi: 10.1021/acsearthspacechem.1c00388

Yoshikawa K, Harada K. 1995. Observations on nearshore pingo growth, Adventdalen, Spitsbergen. Permafrost and Periglacial Processes, 6(4): 361–372, doi: 10.1002/ppp.3430060407

Zhang Jinlun, Spitz Y H, Steele M, et al. 2010. Modeling the impact of declining sea ice on the Arctic marine planktonic ecosystem. Journal of Geophysical Research: Oceans, 115(C10): C10015, doi: 10.1029/2009JC005387

Zhu Zhuoyi. 2022. Clarifying the fate of dissolved organic carbon in turbid glacier meltwater rivers in Svalbard via a series of incubations. Biogeochemistry, 159(3): 337–352, doi: 10.1007/s10533-022-00931-x

Zhu Zhuoyi, Wu Ying, Liu Sumei, et al. 2016. Organic carbon flux and particulate organic matter composition in Arctic valley glaciers: examples from the Bayelva River and adjacent Kongsfjorden. Biogeosciences, 13(4): 975–987, doi: 10.5194/bg-13-975-2016